Self-Assembling Solid Oxide Fuel Cell Materials: Mesoporous Yttria-Zirconia and Metal-Yttria-Zirconia Solid Solutions

Marc Mamak, Neil Coombs, and Geoffrey Ozin*

Contribution from the Materials Chemistry Research Group, Chemistry Department, University of Toronto, 80 St. George St., Toronto, Ontario, Canada M5S 3H6

Received April 19, 2000

Abstract: A new class of mesoporous (nickel/platinum)-yttria-zirconia materials, denoted *meso*-(Ni/Pt)YZ, which may have utility as electrode material in solid oxide fuel cells (SOFCs), have been synthesized by aqueous co-assembly of glycometalates and metal complexes with a surfactant template. These materials form as solid solutions with compositions that can be tuned over the range 12−56 atom % yttrium and 10−30 atom % nickel or 1−10 wt % platinum. The microstructure of the channel wall is nanocrystalline yttria-zirconia (YZ) and nickel/platinum is incorporated as metal oxide/metal clusters with diameters comparable to the size of the pores depending on the degree of loading of the metal precursor. Calcination in air of as-synthesized *meso*-(Ni/Pt)YZ materials causes the channel walls to crystallize and thicken as the imbibed organics are lost. It is the relatively thick, YZ nanocrystalline walls which are believed to be responsible for the impressive 800 °C thermal stability of *meso*-(Ni/Pt)YZ. This new class of binary and ternary mesoporous materials display the highest recorded surface area of any known form of (metal)-yttria-stabilized-zirconia. A narrow mesopore size distribution, nanocrystalline channel walls, and high thermal stability may lead to significant improvements in fuel/oxidant mass transport, oxide ion mobility, electronic conductivity, and charge transfer at the triple-phase-boundary region of SOFC electrodes. It may also enable a reduction in the operating temperature of the SOFC.

Introduction

Despite beginning a new millennium, most of the commercial energy resources remain as they were half a century ago, namely the burning of coal/fossil fuels to generate heat for powering the internal combustion engine. The solid-oxide fuel cell (SOFC) has been a leading candidate for the generation of both stationary and mobile power for the past 10 years.[1] SOFCs operate at elevated temperatures (600−1000 °C) allowing them to process a multitude of fuels including hydrogen, methane, and methanol. The anode has traditionally been a nickel/yttria-stabilized-zirconia (YSZ) cermet while the cathode material is usually a perovskite of the composition $La_xSr_{1-x}MnO_3$ or a platinum/YSZ composite. Electrodes have stringent requirements for use within a SOFC due to the high operating temperatures involved. These include stability in terms of chemical reactivity, phase, morphology, dimensionality, thermal expansion coefficient, catalytic activity, electronic and ionic conductivity, and porosity.[2] Existing electrode materials are intrinsically dense having zero intragranular porosity at elevated temperatures and exhibiting low surface areas arising from intergranular necking produced through sintering processes. Porosity is a singular attribute, which controls not only the transport of gaseous fuel/oxidant to reactive sites but also the length of the triple-phase boundary (TPB) where charge transfer occurs for an electronically conducting electrode.[3−6] The TPB is defined as the interface where the electronically conductive electrode meets both the YSZ electrolyte and the gaseous fuel/oxidant. Both mass transport (gaseous diffusion, adsorption processes, and surface diffusion) and charge-transfer processes at the TPB limit the efficiency of SOFCs. It should be noted that the porosity should not disrupt the percolation of electrons throughout the electrode microstructure.

Several researchers have attempted to improve porosity and enlarge the TPB by manipulating the electrode microstructure through traditional solid-state chemistry and material science techniques, which includes but is not limited to the impregnation of YSZ with noble metal salts and chemical deposition of electrode materials on YSZ substrates.[3−5,7] The common thread among these approaches involves enlarging the TPB by diminishing the dimensions of metal particles such as Ni and Pt in relation to YSZ grains. In essence, these materials are nanoscale or microscale versions of the bulk cermet electrode materials having a comparatively wide pore size distribution with low thermal stability.

The approach described in this paper for synthesizing SOFC electrode materials is novel.[8] It utilizes a soft chemistry strategy in which glycometalates and metal complexes are co-assembled with a supramolecular surfactant template to produce a single phase binary or ternary mesoporous (metal)-yttria-zirconia, denoted *meso*-(M)YZ, which has uniform size mesopores and crystalline channel walls, high thermal stability (800 °C) and electroactive catalytic sites, and potential for high mixed ionic and electronic conductivity. This self-assembly method of making SOFC electrode materials is unique in many respects,

(1) (a) Minh, N. Q. *J. Am. Ceram. Soc.* **1993**, *76*, 563. (b) Ball, P. *Made to Measure, New Materials for the 21st Century*; Princeton University Press: Princeton, NJ, 1997. (c) Steele, B. C. H. *Nature* **1999**, *400*, 619.

(2) Takahashi, T.; Minh, N. Q. *Science and Technology of Ceramic Fuel Cells*; Elsevier: New York, 1995.

(3) Verweij, H. *Adv. Mater.* **1998**, *10*, 1483.

(4) Ziehfreund, A.; Simon, U.; Maier, W. F. *Adv. Mater.* **1996**, *8*, 424.

(5) van Berkel, F. P. F.; van Heuveln, F. H.; Huijsmans, J. P. P. *Solid State Ionics* **1994**, *72*, 240.

(6) Steele, B. C. H. *Solid State Ionics* **1997**, *94*, 239.

(7) Shiga, H.; Okubo, T.; Sadakata, M. *Ind. Eng. Chem. Res.* **1996**, *35*, 4479.

(8) Mamak, M.; Coombs, N.; Ozin, G. *Adv. Mater.* **2000**, *12*, 198.

10.1021/ja0013677 CCC: $19.00
Published on Web 09/02/2000

but the main difference is that a single phase material is created having intragranular porosity, which allows for a high TPB region within a single particle with much improved gas permeability/mass transport qualities. Potentially, *meso*-(M)YZ can increase SOFC efficiency and lower operating temperatures to below 600 °C.

The synthesis of mesoporous materials through surfactant-based self-assembly techniques has been an area of intense research since the discovery of silica-based MCM-41 by Mobil in 1992.[9] As yet, however, there are no adaptations of the technique that produce mesoporous yttria-zirconia analogues that are sufficiently thermal stable to function as SOFC materials.[10] Most mesoporous transition metal oxide materials reported as being stable upon surfactant removal incorporate either phosphate or sulfate groups as stabilizers and to be correct should be regarded as oxo-sulfates or oxo-phosphates. Further, these materials structurally collapse when these groups are removed upon heating to around 400 °C.[11] The only transition metal oxide mesoporous materials free of oxyanion stabilizers and thermally robust were synthesized from metal chloride salts and tri-block copolymer templates, which upon calcination result in mesoporous metal oxides with pores and walls that are larger and thicker than those achievable through surfactant templating. The thicker channel walls most probably lead to the enhanced stability of these materials although mesoporous yttria-zirconia versions were not reported.[10] *meso*-(M)YZ described in this paper is the first example of a thermally stable mesoporous transition metal oxide, produced from templating with a common ionic surfactant, that maintains its structural integrity in the temperature range 400−800 °C. More importantly, *meso*-(M)-YZ is the first example of a mesostructure intentionally designed to be ionically and electronically conductive, and electrocatalytically active for use as fuel and/or oxidant electrode materials in SOFCs.

Herein we report the synthesis and characterization of mesoporous (metal)-yttria-zirconia, *meso*-(M)YZ, solid solutions with compositions that can be continuously tuned over the range 12−56 atom % yttrium and 10−40 atom % nickel or 1−10 wt % platinum. This new class of binary and ternary mesoporous materials display the highest surface area of any known form of yttria-stabilized-zirconia. The nickel and platinum are incorporated into the mesostructure as nanoclusters with dimensions comparable to the size of the pores. The uniform pore structures of these materials are maintained intact up to 800 °C and the channel walls are composed of nanocrystalline yttria-zirconia, which bodes well for their use in solid oxide fuel cells.

Experimental Section

(a) *meso*-YZ: Aqueous Preparation. Zirconium ethoxide (5 g; 99+%, Strem) and 1.66 g of NaOH were added to 50 mL of ethylene glycol (99.9%, Aldrich). This mixture was refluxed overnight under flowing nitrogen to form a clear solution, after which excess ethylene glycol was distilled off creating a thick, clear yellow gel denoted as zirconium glycolate.[12] Separately, 1.2 g of anhydrous yttrium acetate (99.9%, Alfa) was added to 30 mL of ethylene glycol. This mixture denoted yttrium glycolate became clear within 30 min with stirring under nitrogen. The zirconium and yttrium species were then added together in a dropwise fashion forming a much thicker white, gelatinous species denoted YZ glycolate. Typically, $^1/_4$ to $^1/_5$ of this gel was added to a polypropylene bottle containing 30 mL of H_2O, 1 g of cetyltrimethylammonium bromide (CTAB) (Aldrich), and 0.4 g of NaOH. After the mixture was stirred initially for 20 min, each bottle was heated at 80 °C for 1−5 days. The contents of the bottles were recovered by vacuum filtration and were washed with distilled water.

(b) *meso*-YZ: Glycol Preparation. The YZ glycolate was formed as per above. This gel was added to a polypropylene bottle containing 30 mL of ethylene glycol, 1 g of CTAB, and 0.4 g of NaOH. After initial stirring of the mixture, each bottle was heated at 80 °C for 5 days. The bottles were allowed to cool at room temperature forming a very thick brownish coagulation. Hydrolysis was achieved by adding the contents of the bottles to 200 mL of water and a variable amount of NaOH. A powder cake was collected by vacuum filtration and was washed with distilled water.

(c) *meso*-PtYZ: Aqueous Preparation. Sodium hexachloroplatinate(IV), Na_2PtCl_6 (98%, Aldrich), was predissolved in a small amount of water. This yellow solution was then added to a polypropylene bottle containing the mixture prepared in (a) above. The as-synthesized powder cake was black in color and remained black after calcination in air.

(d) *meso*-NiYZ: Aqueous Preparation. Either nickel acetate, nickel nitrate, or nickel chloride was predissolved in warm ethylene glycol. This green solution was then added to a polypropylene bottle containing the mixture prepared in (a) above. The as-synthesized powder cake was green in color and turned black after calcination in air.

(e) *meso*-(M)YZ: Characterization. Powder X-ray Diffraction (PXRD) data were obtained on a Siemens D5000 diffractometer using Ni filtered Cu Kα radiation (λ = 1.54178 Å) with a Kevex 2005-22 solid-state detector. Variable temperature (VT) PXRD data were obtained by using the variable temperature stage attachment. Thermogravimetric Analyses (TGA) were performed on a Perkin-Elmer 7 Series Thermal Analysis System using Perkin-Elmer 7 TAS software version 3.00. All samples were held in a platinum sample holder and were heated under a nitrogen atmosphere at 5 deg/min. Transmission Electron Microscopy (TEM) images were obtained on a Phillips 430 microscope operating at 100 kV. Samples were embedded in an epoxy based resin, cured at 60 °C for 24 h, and sectioned using an ultra-microtome and a diamond knife. The 100 to 300 Å thin sections were then mounted on a copper grid. HR-FE-STEM imaging was done on a JEOL 210F field emission microscope operating at an accelerating voltage of 200 kV. Nitrogen adsorption and desorption isotherms were performed at 77 K. All samples were outgassed at 200 °C. Average pore diameters were determined using the BJH method. Chemisorption in the form of H_2−O_2 titrations was performed. The platinum content of the samples was determined by X-ray Florescence on a Philips 2404, 4 kW sequential XRF. Samples were suspended on 6 μm Mylar film and the Philips Semiquantitative software was used. X-ray photoelectron spectroscopy (XPS) was performed using a Laybold MAX 200 XPS apparatus with Mg Kα radiation. The carbon 1s peak at 285 eV was used for calibration. Mid-IR spectra (4000−400 cm^{-1}) were recorded on a Nicolet 20SXB spectrometer with a resolution of 2 cm^{-1}. Solid samples were pressed into KBr pellets while gel samples sat between two solid NaCl disks.

Results and Discussion

***meso*-YZ.** Both the aqueous and glycol based routes for synthesizing *meso*-YZ demonstrate the ability to a form a solid solution with respect to yttrium and zirconium. Figure 1 shows PXRD patterns of low angle reflections for a series of *meso*-YZ samples containing 12−56 atom % yttrium, which were prepared through the aqueous route. The sample containing 56 atom % yttrium results in a noticeably broader low-angle peak at slightly higher *d* spacings, which may be indicative of less

(9) Kresge, C. T.; Leonowicz, M. E.; Roth, W. J.; Vartuli, J. C.; Beck, J. S. *Nature* **1992**, *359*, 710.

(10) (a) Yang, P.; Zhao, D.; Margolese, D. I.; Chmelka, B. F.; Stucky, G. D. *Nature* **1998**, *396*, 152. (b) Yang, P.; Zhao, D.; Margolese, D. I.; Chmelka, B. F.; Stucky, G. D. *Chem. Mater.* **1999**, *11*, 2813.

(11) (a) Ying, J. Y. et al. U.S. Patent 5,958,367, 1999. (b) Wong, M. S.; Ying, J. Y. *Chem. Mater.* **1998**, *37*, 6470. (c) Antonelli, D. M. *Adv. Mater.* **1999**, *11*, 487. (d) Antonelli, D. M.; Ying, J. Y. *Angew. Chem., Int. Ed. Engl.* **1996**, *35*, 426. (e) Antonelli, D. M.; Ying, J. Y. *Chem. Mater.* **1996**, *8*, 874. (f) Yada, M.; Kitamura, H.; Machida, M.; Kijima, T. *Inorg. Chem.* **1998**, *37*, 6470. (g) Sun, T.; Ying, J. Y. *Nature* **1996**, *389*, 704. (h) Kim, A.; Bruinsma, P.; Chen, Y.; Wang, L.-Q.; Liu, J. *Chem. Commun.* **1997**, 161.

(12) Khushalani, D.; Ozin, G. A.; Kuperman, A. *J. Mater. Chem.* **1999**, *9*, 1491.

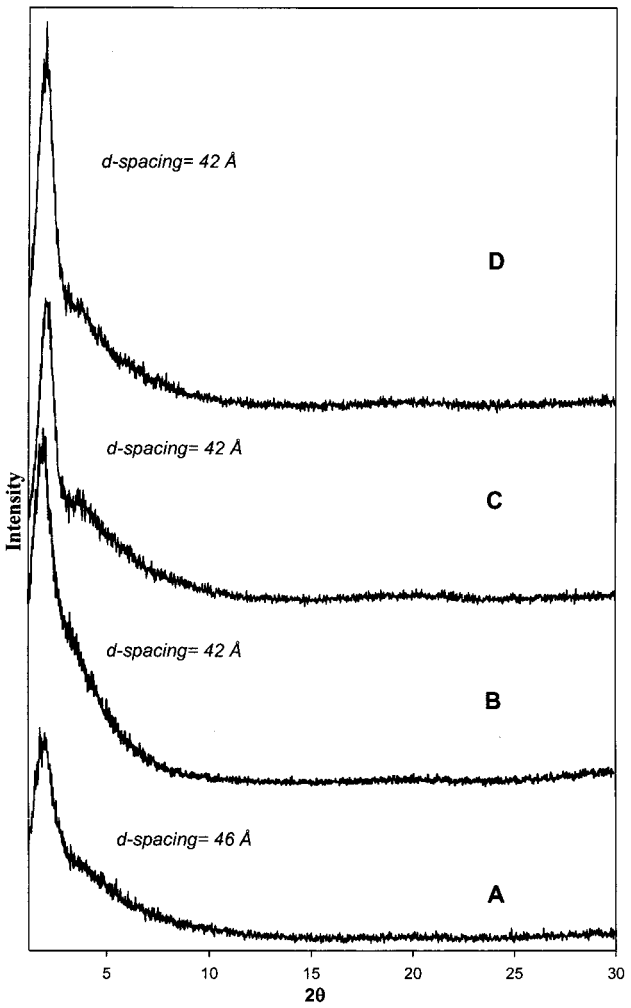

Figure 1. PXRD patterns of *meso*-YZ materials containing the following atom ratios: (A) 0.78 Zr:1 Y, (B) 3.35 Zr:1 Y, (C) 5 Zr:1 Y, and (D) 8 Zr:1 Y. Reprinted with permission from ref 8. Copyright 2000 VCH Publishers.

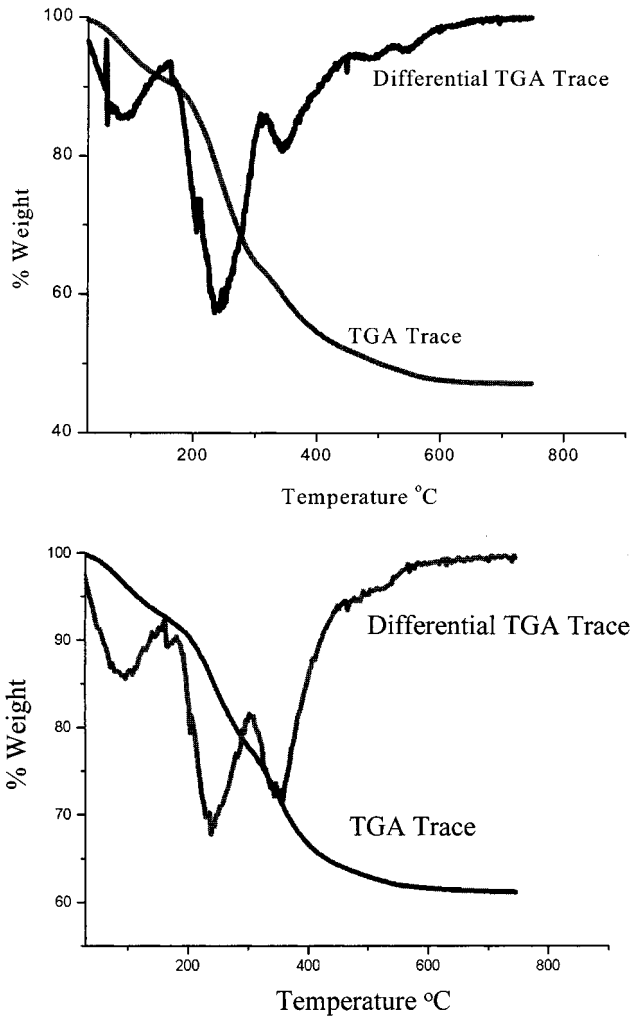

Figure 2. TGA and differential traces for glycol-based *meso*-YZ (Top) and *meso*-YZ (bottom).

ordered mesopores as perceived from extensive comparison of TEM images. A comparison of PXRD patterns of the aqueous and glycol derived as-synthesized *meso*-YZ materials essentially shows no difference between the two materials; however, upon calcination, only the *meso*-YZ derived from the aqueous preparation was deemed to retain a significant portion of the mesostructure from PXRD and gas adsorption analysis.

TGA of *meso*-YZ made under aqueous and glycol conditions demonstrates two significant differences in the as-synthesized material, which give insight into the reason for thermal stability encountered with the aqueous preparation, Figure 2. First, glycol-based *meso*-YZ loses about 16% more mass than that of aqueous-based *meso*-YZ, indicating that the thermally stable *meso*-YZ has less organic constituents in its as-synthesized form. Thus its structure is more fully hydrolyzed and has a higher degree of condensation than its counterpart. The differential weight loss curves show three distinct losses for both materials with the last accounting for the major difference between the two curves. This weight loss occurs just above 300 °C and can be assigned to Y/Zr−OH condensation and/or loss of acetate/glycol groups. Glycol-based *meso*-YZ gives a weight loss of only 3% above 300 °C while aqueous-based *meso*-YZ loses about 13% by mass, indicating that although *meso*-YZ contains less total organic mass within its structure, it is retained until a higher temperature as confirmed through pyrolysis mass spectrometry.

meso-YZ materials demonstrate surprisingly high structural stability upon calcination in air. In fact, *meso*-YZ shows no loss of the low angle PXRD peak intensity up to at least 600 °C as seen in Figure 3. These PXRD patterns are for the as-synthesized and calcined samples containing 30 atom % yttrium (12 h ramp to 600 °C, held for 3 h and then allowed to cool to ambient temperature). As displayed in the inset of Figure 3, reflections corresponding to nanocrystalline yttria zirconia, nc-YZ, begin to emerge upon calcination above 400 °C. These reflections gradually grow in intensity and sharpen upon heating to higher temperatures. As further discussed within the text, a comparison of PXRD, nitrogen adsorption isotherms, and high-resolution field emission-TEM images shows that these higher angle peaks correspond to crystallization of the channel walls with little concurrent reduction of the pore diameter.

TEM analysis of as-synthesized and calcined *meso*-YZ samples confirms the presence of a network of uniform size mesopores, as seen in Figure 4. The pore architecture of these materials is best described as the "worm hole" variety.[13] These kinds of structures, in fact, have been noted in the literature as having advantages for certain applications in terms of greater accessibility to surface sites for gaseous species in, for example, catalysis and adsorption. This is mainly due to the fact that gaseous species in a "worm hole" porous structure can be easily

(13) (a) Tanev, P. T.; Pinnavaia, T. J. *Science* **1995**, *267*, 865. (b) Zhang, W.; Pauly, T. R.; Pinnavaia, T. J. *Chem. Mater.* **1997**, *9*, 2491.

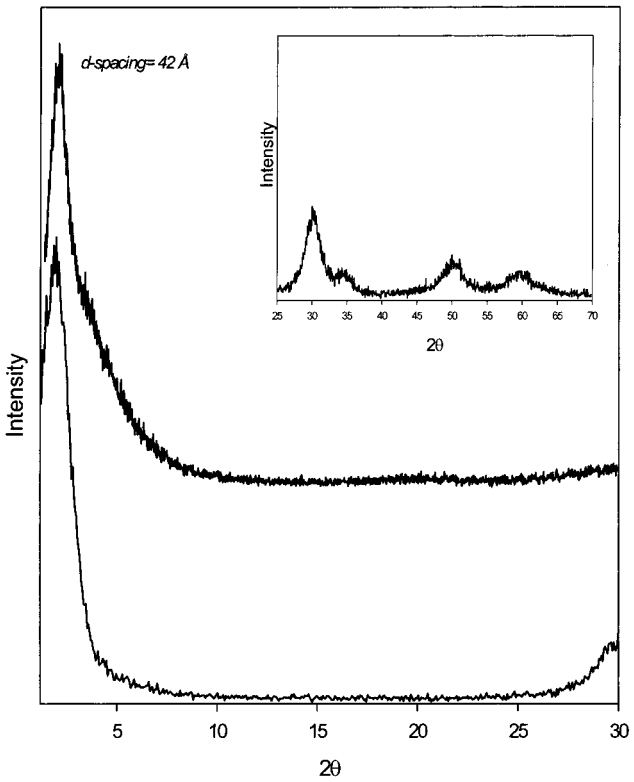

Figure 3. PXRD of *meso*-YZ (3.35 Zr:1 Y) material prepared by the aqueous method: top, as-synthesized; bottom, sample calcined at 600 °C. Inset: High-angle *meso*-YZ peaks. Reprinted with permission from ref 8. Copyright 2000 VCH Publishers.

rerouted to other channels circumventing structural defects, which can disrupt the channel continuity, for instance in the hexagonal array of channels causing blockage to gaseous mass transport. Apart from the pore structure, the calcined *meso*-YZ samples display some variation in contrast giving rise to a "mottled" appearance in TEM images. To rule out the possibility of yttria and zirconia phase segregation, HR-FE-STEM line scans were performed on a sample containing 56 atom % yttrium, which was deemed most likely to contain separate phases as it was previously noted as having the least order as evident from PXRD. A line of 88 nm in length crossing over both light and dark contrast regions was scanned 6000 times across the mesostructured sample. By plotting the intensity of Y and Zr Kα as a function of distance along the line, there appears to be a definite relationship between the two elements as their emission intensities rise and fall in unison ruling out the possibility of separate ZrO_2 and Y_2O_3 domains in the mesostructure. The variation in overall intensity can be most likely attributed to the lack of uniformity in sample thickness achieved through sectioning the sample. Energy-dispersive X-ray microanalysis (EDX) as well as X-ray fluorescence (XRF) confirm the presence of both yttrium and zirconium in all samples and their relative amounts correspond well with the initial stoichiometry of reactants in the synthesis.

The synthesis of a homogeneous binary mesostructured metal oxide can be attributed to the formation of the YZ glycolate gel as a precursor. Major solubility problems have previously plagued yttrium sol−gel chemistry as both the isopropoxide and anhydrous acetate forms have limited solubility in alcohol.[14,15] The higher dielectric constant and coordinating ability of solvents such as ethylene glycol serves to break down the polymeric structure of the yttrium precursor into a useful soluble form to facilitate mesophase synthesis.[15] Through monitoring with IR, the YZ glycolate shows the presence of both glycolate and acetate groups while establishing that the gel is a unique chemical compound and not simply a physical mixture of the yttrium and zirconium glycolates, Figure 5. The IR spectra also show that some acetate and glycolate groups are retained in the as-synthesized *meso*-YZ. Sharp bands in YSZ are seen between 900 and 1000 cm^{-1} and are indicative of asymmetric νZr−O and νY−O stretching modes.[16] These modes are also observed in *meso*-YZ calcined at 450 °C but their line widths are noticeably wider. This may originate from phonon broadening due to the very small dimensions of the yttria-zirconia material contained within the channel wall or inhomogeneous line broadening due to a variety of yttrium and zirconium microenvironments in the channel walls. A micro-Raman spectroscopy study of the *meso*-YZ materials, with a spatial resolution of around 1 μm, has revealed similarly broadened symmetric νZr−O and νY−O modes in the region of 500−600 cm^{-1}. Coexisting in the IR/R spectra are bands in the region of 1500−1600 cm^{-1}, which are attributed to Y/Zr−OH hydroxyls contained in the channel wall of *meso*-YZ.

***meso*-PtYZ and *meso*-NiYZ.** To demonstrate proof-of-concept of our self-assembly synthetic approach to mesoporous yttria-zirconia fuel cell materials, ternary *meso*-MYZ materials have been synthesized by co-assembling platinum and nickel complexes with surfactant templated yttrium−zirconium gels. Figure 6 shows PXRD patterns comparing the as-synthesized and calcined versions of both *meso*-MYZ materials. Calcined *meso*-PtYZ compares well to binary *meso*-YZ in maintaining a narrow low-angle reflection with similar intensity as the as-synthesized material. In comparison, the as-synthesized *meso*-NiYZ material gives a much broader low-angle peak than the binary form, suggesting that it is not as well ordered as *meso*-YZ. Upon calcination, this low-angle reflection grows in intensity and shifts to a higher *d* spacing which is dependent upon the degreee of Ni loading. Both *meso*-MYZ materials exhibit reflections at higher 2θ that correspond to nanocrystalline Pt and NiO.

meso-PtYZ calcined at 400 °C has been examined using in-situ VT-PXRD to probe its thermal and structural stability, Figure 7. Upon heating to 400 °C, the low-angle reflection shifts to slightly lower *d* spacing and grows in intensity implying the formation of a better ordered material with a smaller unit cell. As the temperature increases above 400 °C, the low-angle reflection gradually shifts back to higher *d* spacing corresponding to the formation of a larger unit cell possibly due to a thickening of the nanocrystalline walls. It is only between 800 and 900 °C where the intensity of the low-angle reflection gradually fades. In contrast, the accompanying reflections in the high-angle region of *meso*-PtYZ gradually grow in intensity and sharpen with an increase in time and temperature.

TEM images of calcined *meso*-PtYZ of 2−3 wt % Pt and *meso*-NiYZ of about 15 wt % Ni depicted in Figure 8 reveal clusters that reside within a mesostructure similar in appearance to the binary *meso*-YZ form. It is quite evident from comparison of the two that the *meso*-NiYZ material is somewhat more disordered than the platinum form, which further supports our PXRD analysis. The TEM image of *meso*-PtYZ shows distinctive Pt clusters on the order of 40 Å embedded within a porous network. HR-FE-TEM EDX spot analysis confirms that Pt resides only within these metallic clusters. The observable

(14) Zheng, H.; Colby, M. W.; Mackenzie, J. D. *Mater. Res. Soc. Symp. Proc.* **1988**, *121*, 537.

(15) Hubert-Pfalzgraf, L. G. *New J. Chem.* **1995**, *19*, 727.

(16) Nyquist, R. A.; Kagel, R. O. *Infrared Spectra of Inorganic Compounds: 3800−45 cm*$^{-1}$; Academic Press: New York, 1971.

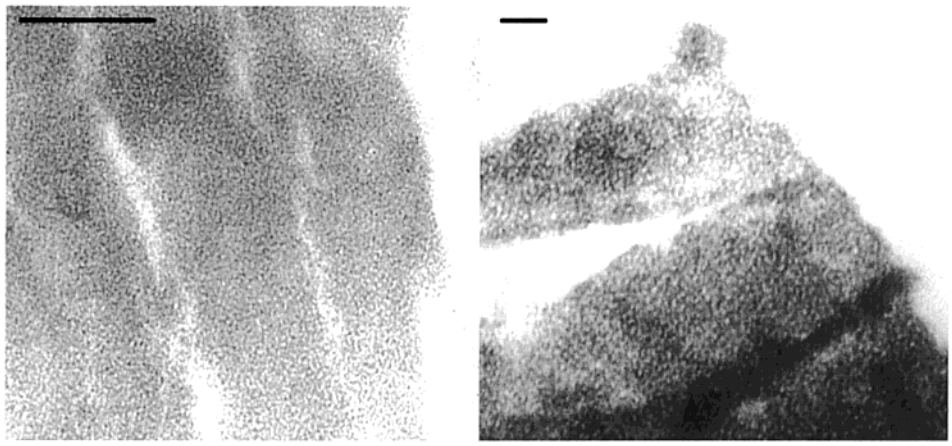

Figure 4. TEM images of a microtomed section of *meso*-YZ materials. Left: As-synthesized 20 atom % yttrium sample; magnification bar = 175 Å. Right**:** 56 atom % yttrium sample calcined at 600 °C; magnification bar = 225 Å. Reprinted with permission from ref 8. Copyright 2000 VCH Publishers.

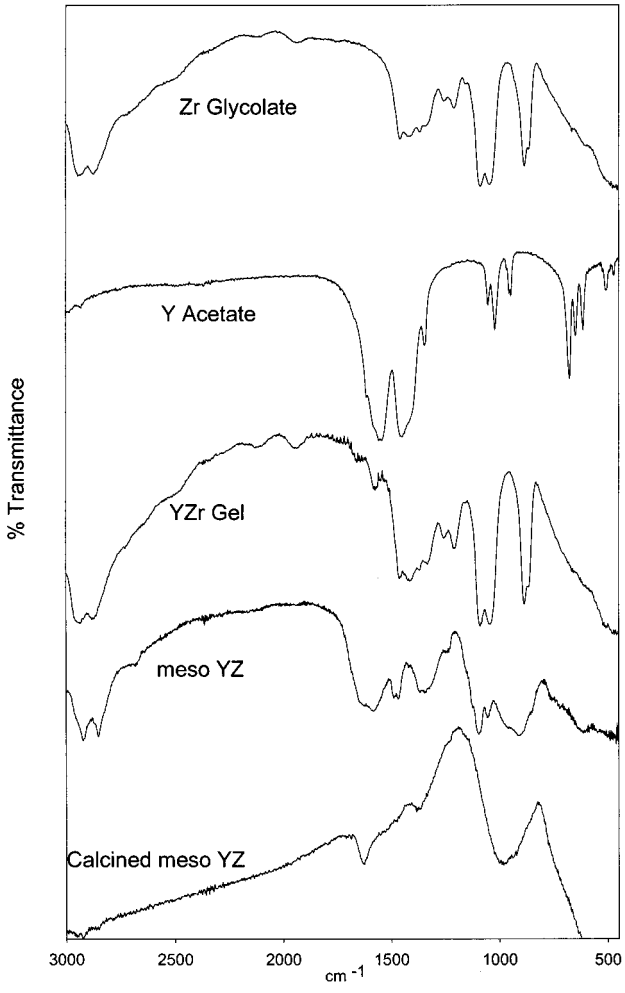

Figure 5. FTIR fingerprint of precursors and products in the synthesis of *meso*-YZ.

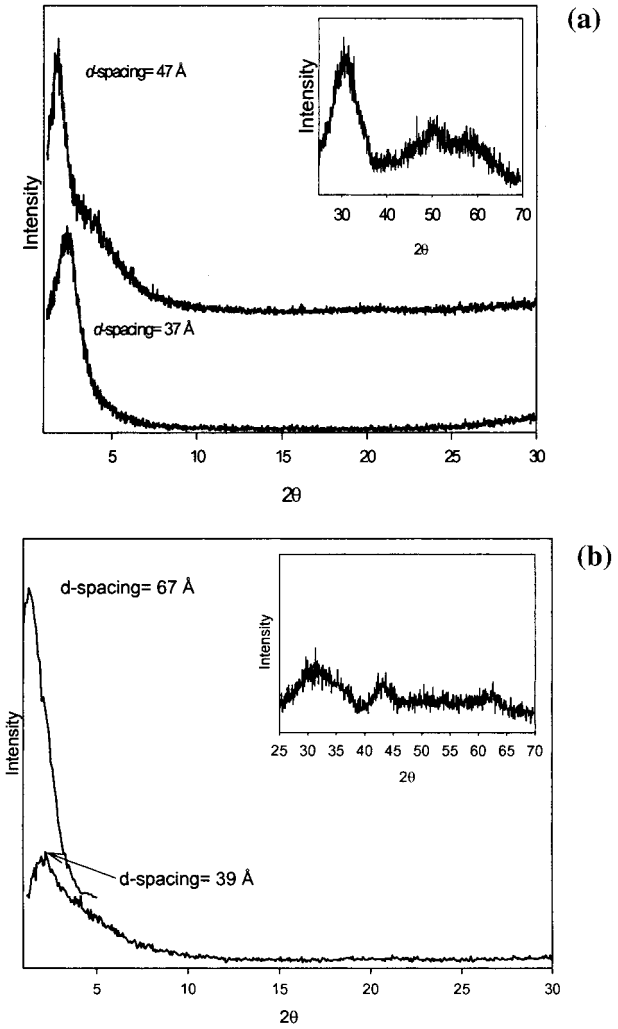

Figure 6. PXRD comparison of as-synthesized and calcined versions of (a) *meso*-PtYZ Bottom trace: Sample calcined to 450 °C and (b) *meso*-NiYZ. Top trace: Sample calcined to 450 °C. Insets: High-angle region.

cluster-like structures in the *meso*-NiYZ section are nanocrystalline NiO_{1+x}. Upon further investigation of a less loaded Ni sample (10 wt %), the microstructure appears more homogeneous and devoid of any cluster-like structures. HR-FE-STEM EDX spot analysis of 30 Å wide areas and SEM EDX mapping shows that Ni, Y, and Zr species coexist throughout the mesostructure suggesting that the NiO_{1+x} phase is finely dispersed throughout the wall structure without any large (>10 nm) phase pure YSZ or NiO_{1-x} domains.

We are currently trying to pinpoint where the Pt clusters reside in relation to the nanocrystalline YZ walls of the mesostructure through microtoming techniques, which would allow for the preparation of ultrathin sections of less than 100 Å. An advantage of imaging these ultrathin sections with HR-FE-TEM is the ability to focus on a single plane of YZ

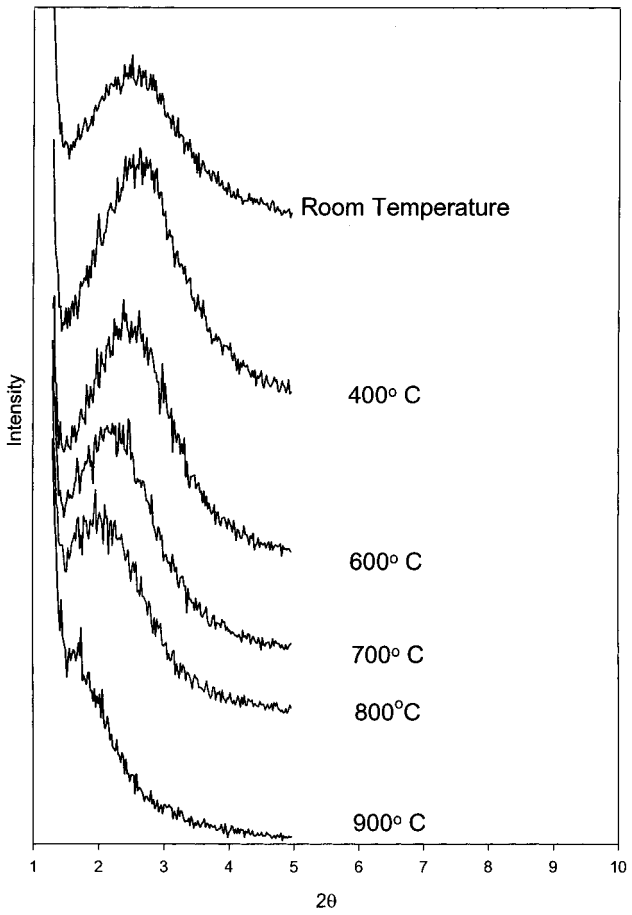

Figure 7. In situ VT-PXRD of *meso*-PtYZ from room temperature to 900 °C.

nanocrystallites and Pt nanoclusters to relate their lattice images to the channel void space. Thin sections of 4−5 times this thickness were far more difficult to interpret because of the superimposing of multiple channels and nanocrystallites within the section. Figure 9 contains a representation of a Fourier filtered HRTEM image where the lattice images of the YZ nanocrystallites show necking between crystallites while a void region representing the pores winds extensively throughout the structure.

Nitrogen adsorption isotherms have been recorded for *meso*-YZ, *meso*-PtYZ, and *meso*-NiYZ, which were calcined at various rates and temperatures in air. Interestingly, all samples yielded isotherms which can be most closely compared to the Type I variety (IUPAC convention, pore diameter <20 Å) with negligible hysteresis; however, upon further inspection it is apparent that our materials continue to adsorb volume up to a p/p^o of 0.3, Figure 10. Each material yielded an average micropore diameter of 17−21 Å, which borders the microporous and mesoporous regimes. Our isotherms may be the result of contributions from both the Type I and Type IV (pore diameter 20−500 Å) isotherms which our material straddles. Additionally, all samples conformed to the Langmuir surface area expression for monolayer coverage yielding linear ln p versus p_o/p plots. Due to the nanocrystallinity of the YZ walls, the diameter of the pores may not be as well defined as those in self-assembled silica-based materials with amorphous walls such as MCM-41. Together with the PXRD/TEM estimated size of the unit cell, the micropore diameter provides an estimate of the wall thickness at about 25−28 Å. One way of rationalizing these results assumes that the framework of the as-synthesized mesostructure is comprised of oligmeric Zr/Y alkoxide species.

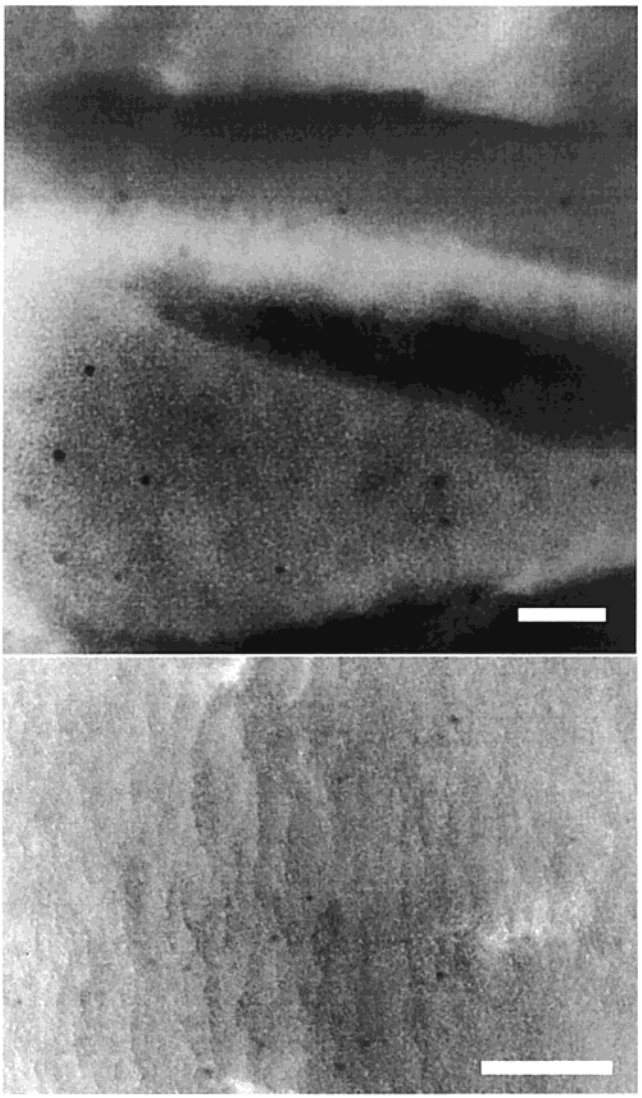

Figure 8. TEM images of microtomed sections of (top) calcined *meso*-PtYZ (magnification bar = 500 Å) and (bottom) *meso*-NiYZ (magnification bar = 575 Å). Top: Reprinted with permission from ref 8. Copyright 2000 VCH Publishers.

They are either weakly connected via bridging acetate/glycolate linkages or behave as discrete units, merely held in place by the templating surfactant mesophase as illustrated in Scheme 1. During the calcination process, thickening of the channel walls of the mesostructure can occur to around 25−28 Å as determined from the combined PXRD/TEM/adsorption results. This may originate from the loss of acetate/glycol groups above 300 °C and concurrent condensation−polymerization of Y/Zr−OH groups to form Zr−O−Zr or Y−O−Zr bonds and a reconstructive transformation of the channel walls of the mesostructure to nc-YZ as seen by VT-PXRD and FE-HR-TEM lattice imaging. Table 1 gives a summary of results for a series of samples (20 atom % yttrium unless stated) in which several trends can be observed. First, the incorporation of low loadings of Pt in *meso*-YZ has a negligible effect upon the overall surface area and pore diameter. Additionally, surface area tends to decrease at higher calcination temperatures and longer heating periods while the average pore diameter remains fairly constant. If one takes into account an invariable pore diameter with an increased d spacing observed from in situ VT-PXRD, it suggests that loss of surface area is resulting from thickening of the channel wall due to crystallization and not collapse of the

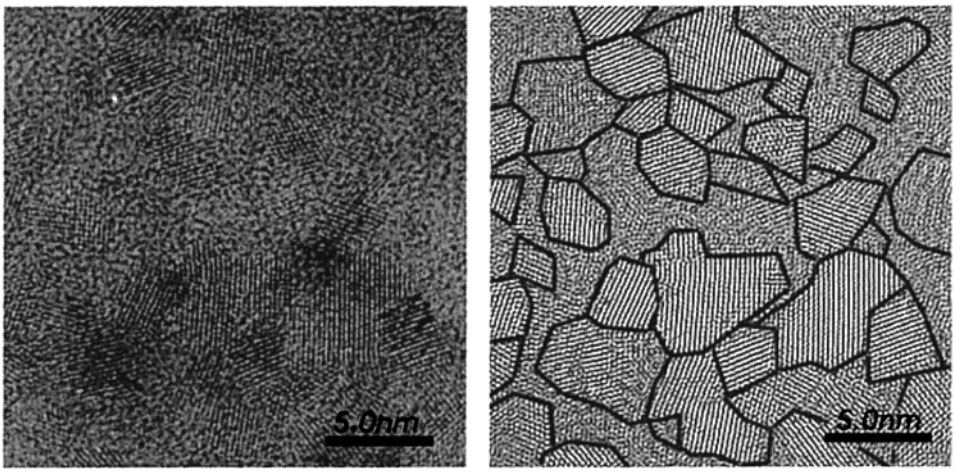

Figure 9. Left: HR−FE−TEM lattice image of calcined *meso*-YZ. Right: Same specimen as in the left only Fourier filtered to enhance the nc-YZ domains which are outlined in black. Magnification bar = 5 nm.

Table 1. Nitrogen Gas Adsorption Data for *meso*-(M)YZ

sample notation	thermal posttreatment	multi-point BET, m^2/g	Langmuir SA, m^2/g	av pore diameter, Å	micropore vol, mL/g
meso-YZ1	6 h ramp to 450 °C	264	353	18.6	0.12
meso-YZ2 (56%Y)	12 h ramp to 600 °C, held for 3 h	116	158	19.2	0.05
meso-PtYZ1	6 h ramp to 450 °C	253	333	18.4	0.11
meso-PtYZ2	12 h ramp to 600 °C, held for 3 h	184	241	18.4	0.08
meso-NiYZ1 (12% Ni)	6 h ramp to 450 °C	156	240	21.2	0.07
meso-NiYZ2 (30%Ni)	6 h ramp to 450 °C	134	235	23	0.06

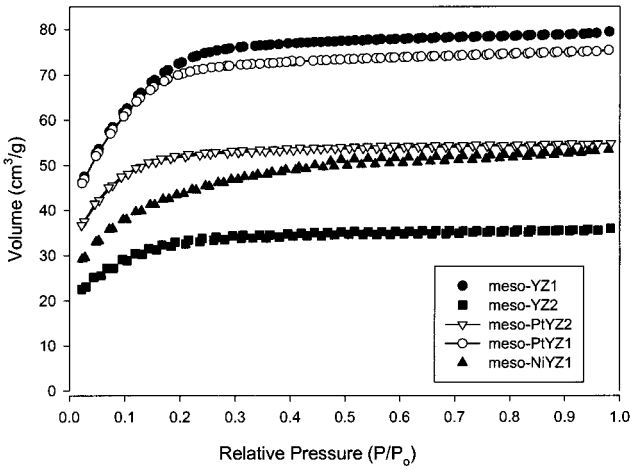

Figure 10. Representative Type I, 77 K nitrogen gas adsorption isotherms of *meso*-(M)YZ materials. Reprinted with permission from ref 8. Copyright 2000 VCH Publishers.

Scheme 1. Self-Assembly of Anionic Yttrium-Zirconium Glycolate and Hexachloroplatinate Precursors with a Supramolecular Cationic Surfactant Template Leading to Formation of a Mesoporous Platinum-Yttria-Zirconia Material Denoted *meso*-PtYZ[a]

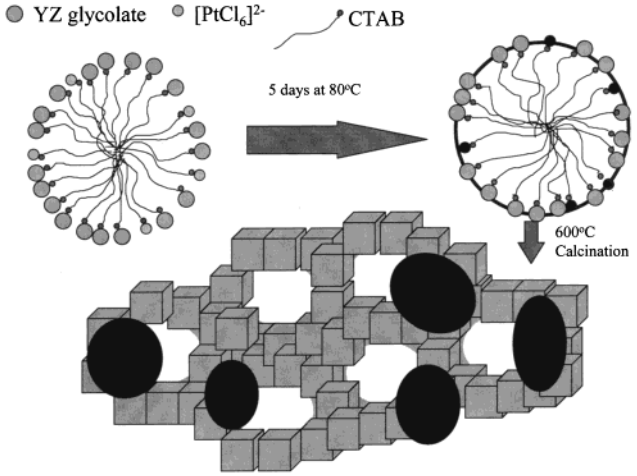

[a] The co-assembled anionic species that comprise the ternary mesophase polymerize via bridging oxide, glycolate, or actetate groups are indicated by the outer black circle. Calcination of the as-synthesized material at 600 °C leads to loss of the surfactant template and formation of a "nanocrystalline mesoporous platinum-yttria-zirconia" composed of cubic YSZ nanocrystallites of about 30 Å, which are depicted as the gray cubes, and Pt nanoclusters of the same order magnitude, which are depicted as the black ovals.

mesostructure. Further support for this hypothesis comes from the fact that the plateau of the adsorption isotherm at high p/p_o remains level with no upturn at highest partial pressures. This is indicative of wholly microporous samples and precludes the presence of either nonporous material or texturally porous material intermixed with microporous *meso*-MYZ. These surface areas are, to our knowledge, the highest recorded for any form of yttria zirconia material and compare quite favorably with microporous zeolites and molecular sieves when the surface areas and pore volumes are converted from a gram to a mole basis per square meter.[4,7,17,18]

Chemisorption experiments were carried out to ascertain the accessible surface sites of the Pt nanoclusters within the *meso*-YZ. A H_2-O_2 titration was performed on three samples of 2.43, 3.06, and 7.4 wt % Pt, which yielded Pt dispersions of 0.183, 0.155, and 0.125, respectively. The fact that Pt is accessible at these high loadings proves the majority of nanoclusters reside within the intragranular mesopore space and are not inaccessibly occluded within a matrix of YSZ. These dispersions give surface-weighted average crystallite sizes of 61.8, 72.8, and 90.5 Å, which are the same order as those estimated from the TEM/PXRD analysis. The slight difference may be due to chemisorption induced Pt agglomeration and/or inaccessible Pt surface sites where attached to the YZ framework.

The nature of the nanocrystalline walls in *meso*-YZ was further examined through PXRD and TEM. PXRD shows the higher angle region of the as-synthesized material to have a mainly amorphous channel wall material which becomes nanocrystalline in the calcined material (600 °C). Upon further examination of *meso*-PtYZ, the reflections of the nanocrystalline wall material match well with cubic YSZ (JCPDS No. 30-1468) and metallic platinum (JCPDS No. 04-0802). Micro-Raman spectroscopy supports our determination for the presence of the cubic YSZ phase over the tetragonal phase. By applying the Scherrer equation to diagnostic peaks for a *meso*-PtYZ with a relatively high loading of Pt (6−8 wt %), the particle size was estimated to give the following values: cubic YSZ-111 peak, 35 Å; 220 peak, 29 Å; metallic Pt-111 peak, 69 Å; and 200 peak, 58 Å. The cubic YSZ compares well with our estimation of both channel wall thickness 25−28 Å and the size of the platinum nanoclusters from a less loaded sample, estimated from TEM to be about 44 Å. This agreement is acceptable since higher loadings of Pt lead to the formation of larger nanoclusters, and in addition, the Pt peaks partially overlap with cubic YSZ, which creates difficulty in obtaining true fwhm values. Furthermore, the nc-YSZ domains are on the order of 30 Å, which supports our PXRD/gas adsorption estimate for channel wall thickness as well as our particle size estimation from the Scherrer equation. *meso*-NiYZ consists of both nanocrystalline YSZ and NiO_{1+x} (JCPDS No. 02-1216) phases although a reliable particle size of NiO_{1+x} could not be ascertained due to overlap of the 111 reflection with the 200 of the YSZ as well as an extremely broad 200 NiO_{1+x} reflection. The optical properties of *meso*-NiYZ suggest it consists of p-doped nonstoichiometric NiO_{1+x}, which we believe is located as nanocrystallites within the YZ wall structure. Evidence for this is manifested in the low-angle PXRD reflection, which experiences an increase in *d* spacing upon calcination and varies accordingly with the amount of NiO_{1+x} incorporated in the initial synthesis, i.e., higher Ni content leads to higher *d* spacing. It is during the calcination process where the Ni(II) precursor oxidizes and crystallizes into the YZ walls leading to a dramatic thickening of the walls not seen for *meso*-YZ devoid of Ni. The thick YZ/NiO composite walls are the most likely reason for lower BET surface areas than our other materials.

X-ray photoelectron spectroscopy (XPS) establishes the presence of zerovalent Pt(0) as the major species in both the as-synthesized and calcined materials.[19] We believe the Pt(IV) precursor complex is reduced over a period of 3 to 4 h, perhaps after the $PtCl_6^{2-}$ species co-assembles with the cationic surfactant cetyltrimethylammonium bromide, CTAB, and the YZ glycolate species to form *meso*-PtYZ as illustrated in Scheme 1. Ample evidence for the reduction of noble metal salts at low temperatures through the oxidation of ethylene glycol exists in work by Figlarz and co-workers, who coined this reaction the "polyol process".[20] Elemental analysis by XRF and XPS corroborates the expected elemental composition of *meso*-PtYZ as evident from Table 2. Since both bulk and surface analytical techniques give similar values, it can be inferred that *meso*-PtYZ has compositional homogeneity throughout the sample.

Table 2. Elemental Analysis Data for *meso*-(M)YZ

	Pt %	Y %	Zr %
expected	1−2	19.7	80.3
XPS	1.6	18.3	81.7
elemental anal	1.1	19.9	80.1

Conclusion

Thermally robust mesoporous (nickel/platinum) yttria zirconia materials, with high surface area, narrow pore size distribution, and nanocrystalline channel walls, have been synthesized using a soft chemistry self-assembly strategy. The approach is based upon the co-assembly of a supramolecular cationic surfactant template: yttrium-zirconium glycolate and nickel(II) or platinum(IV) complexes. This synthetic strategy yields compositionally homogeneous mesoporous yttria-zirconia in which nanoscale nickel oxide or platinum metal clusters are uniformly dispersed throughout the material. Upon calcination of the as-synthesized material, surfactant template is removed and a reconstructive structural transformation occurs leading to a porous material with nanocrystalline YSZ channel walls, a narrow pore size distribution, and surface areas which to our knowledge are the highest yet observed for any form of yttria-stabilized-zirconia. The large surface area and high thermal stability of *meso*-(Ni/Pt)YZ bode well for its possible use as a fuel and/or oxidant electrode material in SOFCs.

Acknowledgment. G.A.O. is deeply indebted to Mobil Technology Company for financial support of this work. We would like to thank Dr. R. Sodhi of the Biomaterials Department for assistance with X-ray photoelectron spectroscopy, Dr. Mike Gorton of the Geology Deptartment for assistance with X-ray Fluorescence spectroscopy, McMaster University Powder Processing Facility for gas adsorption measurements, and especially Prof. Albert Vannice and Willy Rachmady of Pennsylvania State University for chemisorption measurements.

JA0013677

(17) Breck, D. W. *Zeolite Molecular Sieves*; John Wiley and Sons, Inc.: New York, 1974.

(18) (a) Alvarez, M. R.; Torralvo, M. J. *Colloids Surf. A: Physicochem. Eng. Aspects* **1996**, *113*, 165. (b) Kim, J.; Lin, Y. S. *J. Membr. Sci.* **1998**, *139*, 75.

(19) Hino, M.; Arata, K. *Appl. Catal. A: General* **1998**, *169*, 151.

(20) (a) Fievet, F.; Lagier, J. P.; Blin, B.; Beaudoin, B.; Figlarz, M. *Solid State Ionics* **1989**, *32/33*, 198. (b) Ducamp-Sanguesa, C.; Herrera-Urbina, R.; Figlarz, M. *J. Solid State Chem.* **1992**, *100*, 272.